Saturation ratio influence on perforation and penetration of concrete subjected to missile impact: a DEM approach

Abdallah Accary, Hicham Benniou, Yann Malecot, Matthieu Briffaut, Laurent Daudeville

Noname manuscript No.
(will be inserted by the editor)

Saturation ratio influence on perforation and penetration of concrete subjected to missile impact: a DEM approach

Abdallah Accary[1] · **Hicham Benniou**[1] · **Yann Malecot**[1] · **Matthieu Briffaut**[1] · **Laurent Daudeville**[1*]

Received: date / Accepted: date

Abstract Concrete structures are widely used as shielding barriers to protect sensitive infrastructures. Possible accidental conditions such as aircraft impacts on nuclear containments, have led to an increasing demand for advanced design of concrete structures under extreme loading. Several studies have shown that the presence of free water in concrete significantly affects its response when subjected to static loading with high mean stresses or dynamic loading with high strain rates. Therefore, the aim of this paper is to investigate the influence of the saturation ratio on perforation and penetration of concrete. To achieve this purpose, the study will simulate the impact of ogive-nosed steel projectile on three plain concrete targets, passively confined by means of steel jackets surrounding the cylindrical specimens.

Keywords Discrete element model · Impact · Concrete · Water saturation ratio · Strain rate effect

1 Introduction

The safety and protection of sensitive infrastructures under severe dynamic loading, such as earthquakes and impacts, is an important topic of study in the field of civil engineering. The partial or complete failure of these structures, such as nuclear power reactors, dams, and high-rise buildings, poses a significant threat to human life. A massive concrete structure subjected to the impact of a rigid projectile undergoes three successive damage phases: cratering on the front face of the structure associated with simple tension, dynamic compression during projectile penetration, and spalling on the rear face depending on projectile velocities and target thickness [40], [24], [9], [15]. To better understand complex phenomena such as brittle damage, compaction under very high confining pressure (up to 650 MPa), and the strain-rate effects, multiple experimental studies have been conducted on widely investigated R30A7 concrete (σ_c = 30 MPa at 28 days). Previous studies aimed to understand the effect on the concrete behavior under quasi-static conditions of the loading path [19], [20], [38], [12], [25], of saturation and water-to-cement ratios [37], of coarse aggregates shape and composition [30], [31], of initial matrix porosity [26], and of water interstitial pore pressure [1]. Spalling experiments were also performed to evaluate the high strain-rate tensile strength of concrete [13], [15].The results have proved that the unconfined compressive strength is a poor indicator of the high-pressure mechanical response of concrete, and that the water saturation ratio is an important parameter governing the triaxial compressive strength of concrete. Furthermore, the authors have noted that pore pressure could be of the order of the confining pressure under hydrostatic test at 400 MPa. For the investigation of concrete behavior under dynamic loading, missile impact tests were performed on plain concrete targets of $300mm$ and $800mm$ in thickness using the same type of concrete mixture [32]. Many finite element models were proposed to simulate phenomena occurring during missile impact: brittle damage in tension, pore closure under high triaxial stress, and strain rate effects ([27], [33], [6], [23]). These finite element models demonstrated a good capacity to reproduce the pre-failure behavior but a limited ability to describe severs damages such as fragmentation mechanisms at the macro scale. In addition, such fi-

*Corresponding author: Laurent Daudeville
E-mail: laurent.daudeville@univ-grenoble-alpes.fr
[1]Univ. Grenoble Alpes, CNRS, Grenoble INP, 3SR, 38000 Grenoble, France

nite element models are based upon an erosion criterion that has no physical sense and that must be identified for each test. A 3D Discrete Element Method (DEM) model was developed by Daudeville et al. [2], [18], [36] to simulate the penetration test, but the effect of saturation ratio was not taken into consideration. Only a few finite element models accounted for the influence of the saturation ratio on the response of concrete targets under impact ([6], [17], [3], [39]). The aim of this paper is to present a new DEM model implemented in the open-source code YADE [22] that can reproduce the behavior of concrete targets under impact loading including the effect of water saturation ratio. To achieve this, specific interaction laws between discrete elements (DE) were developed and validated under quasi-static compression at very high confinement pressure under both dry and very wet conditions [5]. The perforation and penetration tests performed on wet targets are simulated with the new DEM model and results are compared with the experimental data.

2 Concrete Model

2.1 Constitutive model description

The constitutive DEM model implemented in this study was validated, at the macroscopic scale, through numerical simulations of triaxial tests on R30A7 concrete at very high confinement pressures under quasi static conditions [5]. Each spherical DE has 6 degrees of freedom (DOF) (3 translations, 3 rotations). Under impact, concrete material experiences high levels of stress, leading to irreversible strain such as compaction. To capture this behavior, the model includes six nonlinear interactions between DE. These six interactions correspond to tension-compression, shear (2 directions) and involve the translation DOFs as well as torsion and bending (2 directions) that involve the rotation DOFs (see [5] for further details). Moreover, since the saturation ratio of concrete affects its behavior significantly, the model incorporates a dependency between the water saturation ratio and the inelastic deformation caused by pore closure. Table 1 shows the constitutive behavior parameters identified thanks to simulations of quasi-static tests. Figures 1 and 2 demonstrate the model's ability to replicate the experimental behavior of concrete under high confining pressure (up to 650 MPa) in both dry and very wet states.

Table 1 Model parameters calibration values (see [5] for details)

Parameters	Physical meaning	Values
E (GPa)	Young modulus	30
ν	Poisson ratio	0.2
ϵ_0	Limit elastic stain in tension	$1e^{-4}$
ϵ_f	Limit failure strain	$20\epsilon_0$
ϕ_c (radians)	Contact friction angle	0.8
C_0 (MPa)	Shear cohesion	4
k_p	Strain hardening modulus	2
k_h	Consolidated material parameter	1
ϵ_{el}	Limit elastic strain in compression	$20\epsilon_0$
ϵ_{pl}	Maximum compaction strain	$200\epsilon_0$
λ_{100}	Saturated sliding threshold coefficient	1
λ_0	Dry sliding threshold coefficient	5

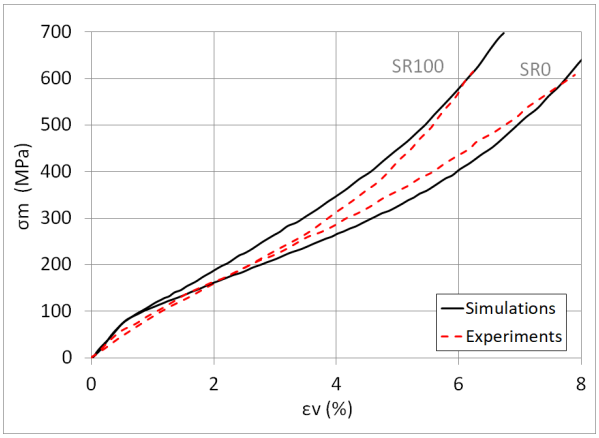

(a)

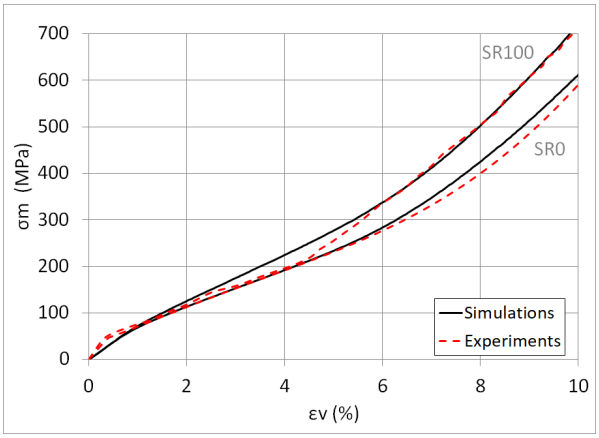

(b)

Fig. 1 Stress-strain curves: simulation vs. experimental results [37]. **a** hydrostatic, **b** oedometric under dry and wet states [5]

2.2 Strain rate and saturation ratio effects

To accurately model the dynamic response of concrete structures under impact, the model must account for

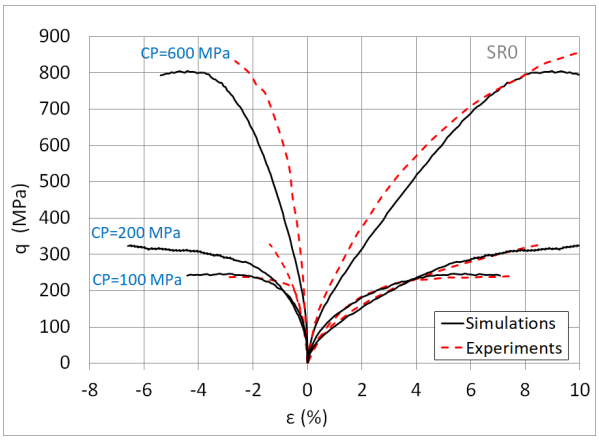

(a)

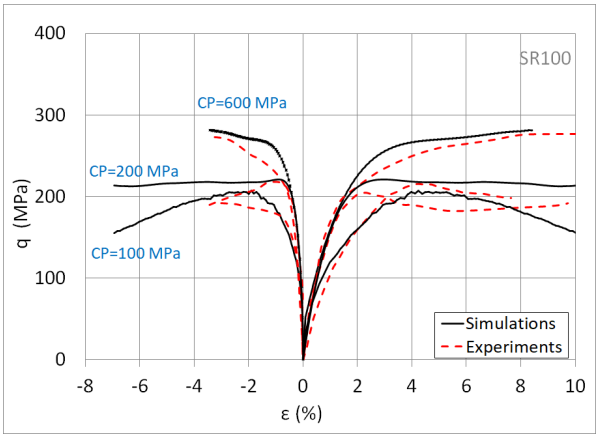

(b)

Fig. 2 Stress-strain curves: simulation vs. experimental results [37]. Deviatoric phase of triaxial test under **a** dry, **b** wet states [5]

the strain rate effects in the concrete behavior. Results of tests performed with Split-Hopkinson pressure bars have shown that both the apparent tensile and compression strength increase as the strain rate ($\dot{\epsilon}$) increases [35], [13]. However, this increase remains more pronounced in tension: the resistance of concrete is 5 to 7 times greater for dynamic test than for quasi-static test [28]. In compression, the resistance of concrete is at maximum 2 times greater for dynamic tests than for quasi-static tests [7]. In other words, the ratio of dynamic strength over static strength (called dynamic increase factor DIF) appears to be much more higher in tension than in compression. It is generally accepted that the increase of apparent compression strength with strain rate is due to inertial effects, as reported by [10], [11]. Hentz [21] showed numerically that the strength increase in dynamic compression is a structural effect. Therefore, only the strain rate effect in tension is taken into account in this study. This is achieved by modifying the tensile resistance between DEs using equation 1 inspired from CEB (Euro-International Committee of Concrete [8] formulation: where f_t is the dynamic tensile strength, $f_{t,static}$ is the static tensile strength and ϵ_{static} is the reference static strain rate set equal to $10^6 s^{-1}$.

The effect of saturation ratio on the concrete tensile strength at high strain rate was also studied by [34] and [17]. They showed that concrete resistance is more sensitive for wet samples at high strain rate than for dry samples. Therefore, numerical simulations of impact test on dried and saturated concrete are performed to investigate the saturation ratio effect at the structural scale. Table 2 describes the values of the recommended parameter values that were calibrated for both dry and saturated concrete. Figure 3 shows the identified and experimental DIF values as function of the strain rate, with both dry and saturated concrete maximum values set equal to 5.

$$DIF = \frac{f_t}{f_{t,static}} = \begin{cases} 1 & \text{if } \dot{\epsilon} \leq \dot{\epsilon}_{static} \\ (\frac{\dot{\epsilon}}{\dot{\epsilon}_{static}})^{\alpha\delta_1} & \text{if } \dot{\epsilon}_{static} \leq \dot{\epsilon} \leq 1 \\ e^{(6\delta_1 - 2)(\frac{\dot{\epsilon}}{\dot{\epsilon}_{static}})^{\delta_2}} & \text{if } 1 \leq \dot{\epsilon} \end{cases} \quad (1)$$

Table 2 Model parameters calibration for saturated and dry concrete conditions

Parameters	α_1	δ_1	δ_2
Saturated	1.5	1/30	1/3
Dry	0.75	1/30	0.1

3 Penetration test setup and experimental results

A campaign of experimental tests was conducted by CEA-Gramat in 2009. A 2.4kg, $52mm$ in diameter and $300mm$ in length ogive nosed steel penetrator (Fig. 4(a)) was launched on cylindrical ($\Phi = 800mm$) R30A7 unreinforced concrete targets using the gas launcher DEIMOS (Fig. 4(b)). This launcher allows tests to be performed at different striking velocities (ranging from 225 to $425m/s$). An accelerometer was embedded within the projectile to measure the axial deceleration (Fig. 4(b)), and a high-speed video camera was used to observe the interaction between the projectile and the

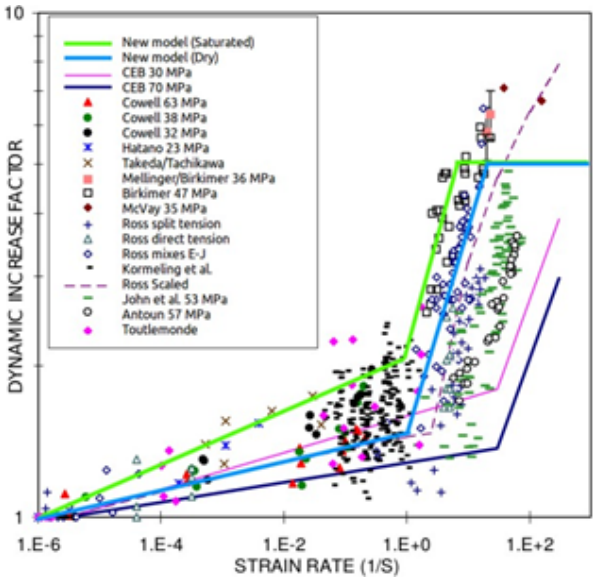

Fig. 3 New proposed model's DIF values as a function of strain rate for dry and saturated R30A7 concrete compared to experimental results and other models [29]

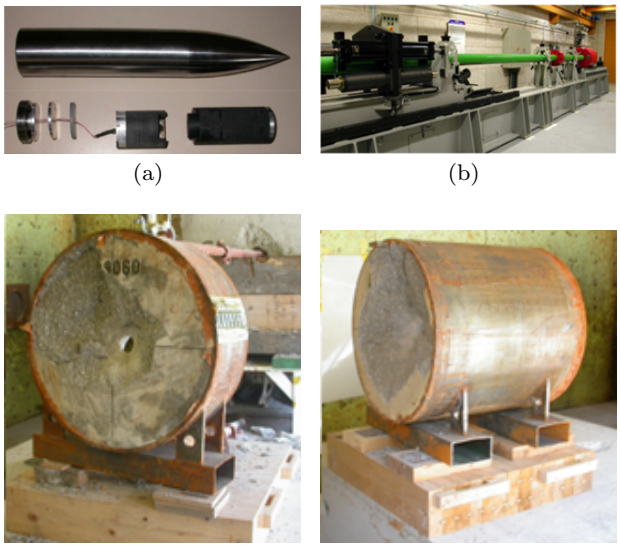

Fig. 4 Experimental tests: **a** ogive nosed steel penetrator, **b** gas launcher, **c** perforation concrete target (H300m), **d** penetration concrete target (H800mm) [6]

concrete target. Once the test was performed, a topographic laser system was used to measure the dimensions of the crater and tunnel regions. The concrete targets were confined with 15 mm steel ring and held in water until the tests were performed; thus, the targets were fully saturated [4]. Figures 4(c) and 4(d) illustrate the damage of the two faces of the target after the perforation and penetration test, respectively. The main parameters of each impact test are gathered in Table 3. Figure 5(a) shows the velocity profile for test 1 only. Figure 5(b) depicts the penetration depth profiles of the three tests: test1 perforated the concrete target (PD $\geq$ H300mm), while tests 2 and 3 only penetrated the concrete targets (PD $<$ H800mm).

Table 3 Tests parameters: experimental data

Parameters	Test 1	Test 2	Test 3
Height H (mm)	300	800	800
Initial Velocity V_i (m/s)	333	347	227
Residual Velocity V_r (m/s)	93	–	–
Penetration Depth PD (mm)	$\geq$300	268	193
Front face crater diameter FD (mm)	400	700	400

4 Simulation setup

The projectile is represented by a single (DE) clumped inside a non-deformable shell of facets that represent its contour. The density of this single DE is calculated to be representative of the actual mass of the projectile. This hypothesis allows reducing the number of DEs in the simulation. Figure 6 shows the designed projectile, which is considered to behave as a rigid body. A frictional interaction law is used to model the concrete target-projectile interaction. Calculations showed that the friction angle has a slight influence on the projectile's behavior. However, as the real friction angle between the projectile and the concrete target cannot be determined experimentally, it was set to be equal to zero, providing acceptable results. Two cylindrical specimens, both with a diameter of 800mm, but different heights, were generated to represent the concrete target for tests 1, 2, and 3. One specimen was 300mm in height and made up of 140,000 spheres, while the other was 800mm in height and made up of 385,000 spheres as shown in Figures 7(a) and 7(b) respectively. A layer of (DEs) was added to the lateral face of each specimen to represent the confinement steel jacket. The DEs in this layer were blocked in translation and rotation. The interactions between DE were not orientated in any privileged directions, and the isotropy of orientations can be checked by plotting the cumulative orientation distribution of interactions (Figures 7(a) and 7(b)). The numerical compacity of the medium is around 0.6 and the interaction radius I_r is set equal to 1.5 so that an average of 12 interactions per element is obtained. to ensure the isotropy of interactions orientations [2].

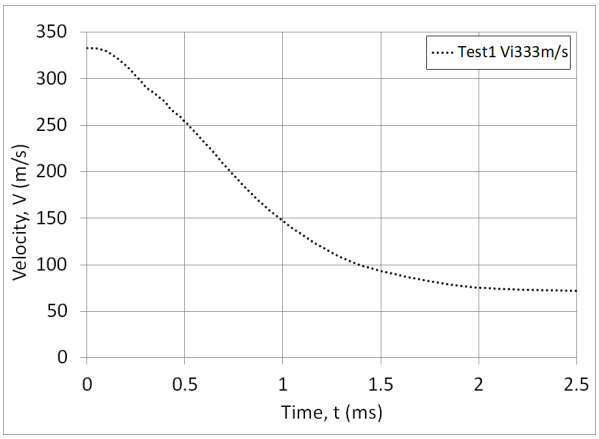

(a)

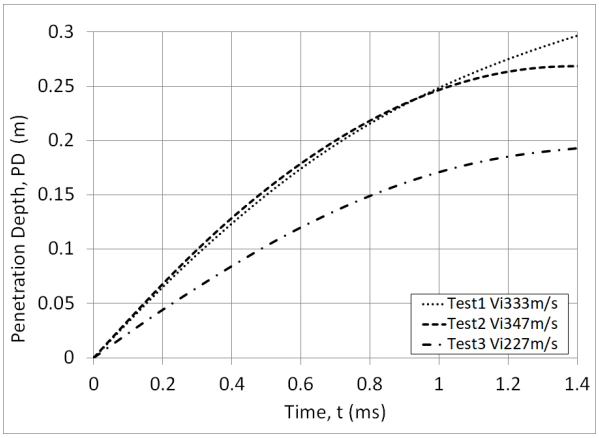

(b)

Fig. 5 Penetration tests result: **a** Velocity vs time, **b** Penetration depth vs time [32]

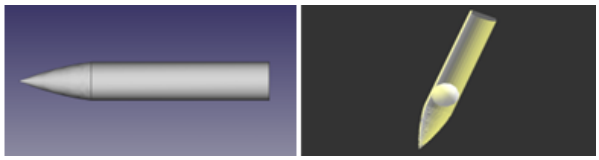

Fig. 6 Projectile design: 3D modeling in YADE

5 Simulation results (case of saturated sample)

The three tests described in (sec. 3) were simulated using the numerical samples under saturated condition (see Table 2). The projectile velocity and penetration depth in each simulation were computed and compared to the available experimental data, as presented in Table 4).

In the perforation **test 1** ($V_i = 333m/s$ on H300mm target) a good correspondence can be observed between simulation and experimental results in terms of velocity and penetration depth profiles (Figs. 8(a), 8(b)). Nevertheless, a delay of 0.16ms is recorded between the simulation and experimental results once the perforation

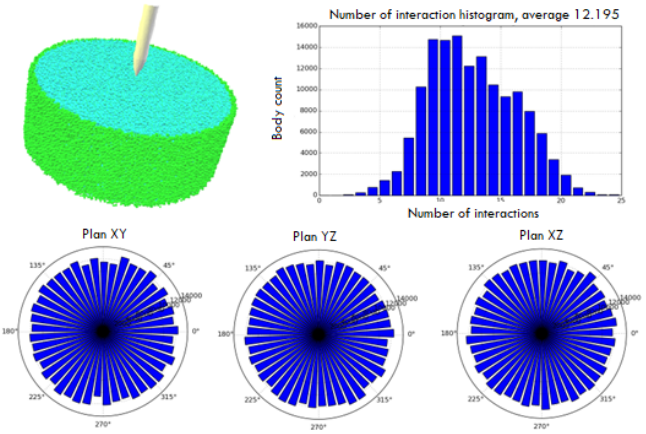

(a)

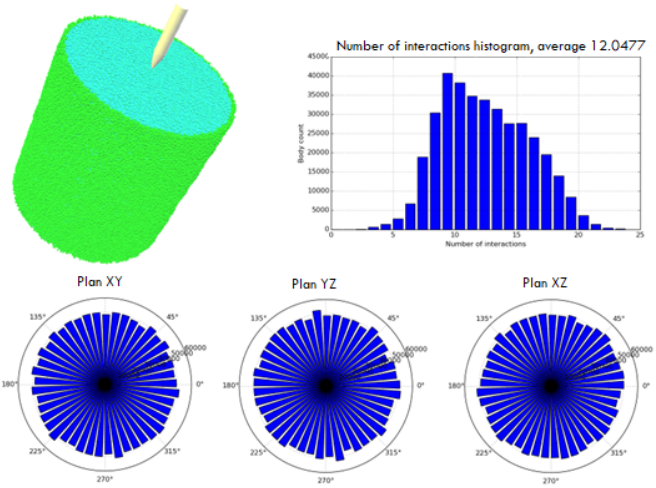

(b)

Fig. 7 Concrete target model in YADE: histogram of interaction number for each DE, and initial distribution of interaction links' orientation in the numerical sample **a** H300mm, **b** H800mm

Table 4 Comparison between experimental and simulation results at T = 1.4ms

Parameters	Test 1 Sim./ Exp.	Test 2 Sim./ Exp.	Test 3 Sim./ Exp.
Height H(mm)	300	800	800
V_i (m/s)	333	347	227
V_r (m/s)	93/94	–	–
PD (mm)@1.4ms	> 300	253/268	198/193
FD (mm)	400/400	700/700	400/400

occurred. Post-processing shows that during the first 0.3ms, corresponding to the penetration phase, damage develops in vicinity of the projectile nose and only on the front face of the concrete target. Starting from 0,5ms conical fracturing appears on the front face near

the projectile, and damage appears on the rear face of the target (Fig. 9). The topology of the numerical sample after perforation is shown in Fig. 10(a). The blue area indicates that the links between DEs in this part of the specimen are damaged either completely or partially, forming small chunks that are detached from the target. A good agreement between numerical and experimental results is observed in terms of penetration depth and both front/back face crater dimensions (Fig. 10(b)).

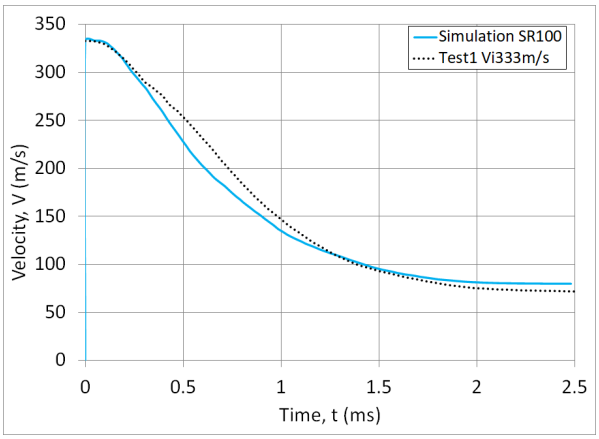

(a)

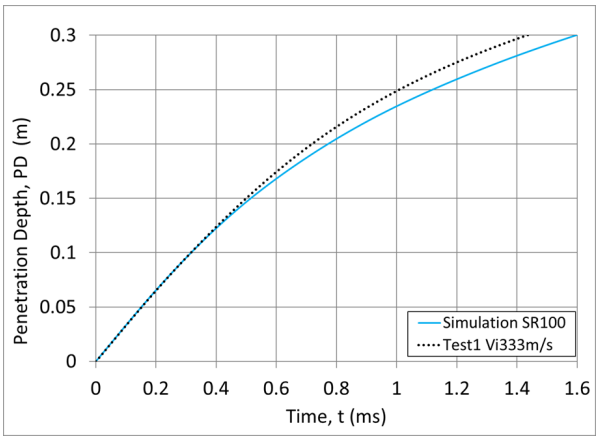

(b)

Fig. 8 Test 1 comparison between experimental and simulation results for saturated concrete **a**, velocity **b** penetration depth profiles

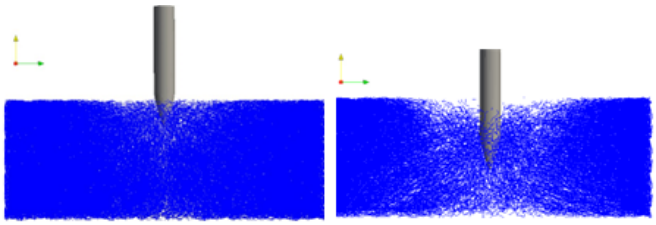

Fig. 9 Test 1 damage in the H300 mm concrete target **left** at $0.3ms$ **right** at $0.5ms$

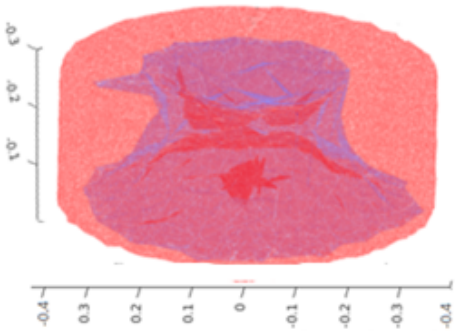

(a)

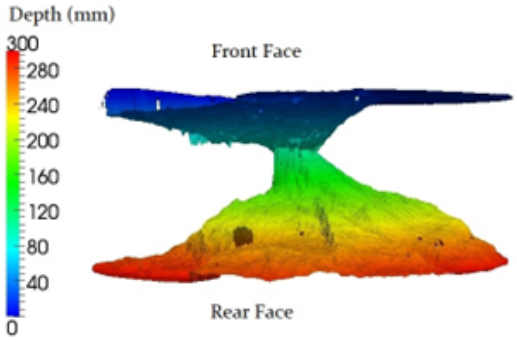

(b)

Fig. 10 Test 1 topology of the target after impact **a** 3D numerical view, **b** experimental view

In both penetration **tests 2** and **3** ($V_i = 347m/s$ and $227m/s$ respectively on H800mm target), the simulation results closely matched the experimental results in terms of penetration depth profiles (Fig. 11). For **test 2**, the difference between the final numerical depth and the experimental depth is only $15mm$ at $1.4ms$. Note that the projectile stopped at $2.4ms$ in the simulation. **Test 3** exhibited almost perfect replication of the experimental penetration depth in the numerical simulation, with only a $5mm$ difference between the two curves at $1.4ms$ (see Table 4). Figures 12(a) and 12(b) show the topology of the numerical sample after penetration compared to the experimental one for **test 2**. The blue area indicates that the links between DEs are damaged, the fracture remains localized inside the tar-

get. No cratering is noted on the rear face, where approximately 33% of the concrete target height has been penetrated.

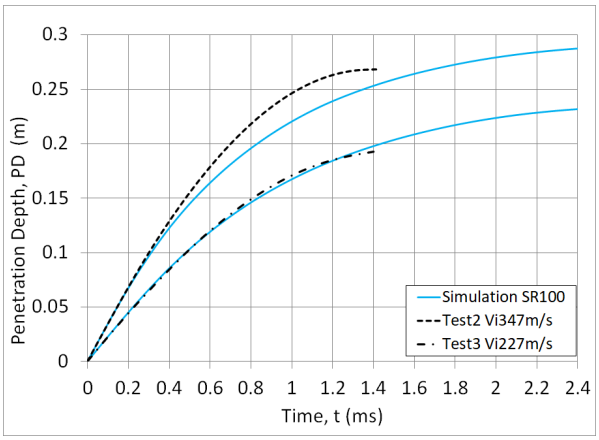

Fig. 11 Tests 2 and 3 comparison between experimental and simulation results for saturated concrete: penetration depth profiles

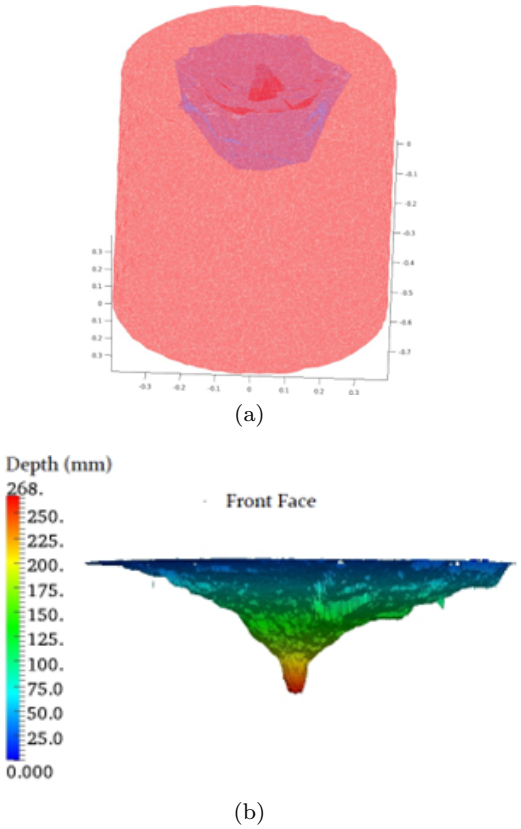

Fig. 12 Test 2 topology of the target after impact **a** 3D numerical view, **b** experimental view

6 Saturation ratio effect

In order to investigate the effect of free water content on the penetration of rigid projectile in concrete targets, **tests 1, 2** and **3** described earlier were also replicated on dry R30A7 concrete. As stated in sec.2.2, the parameters identified on dry sample were applied on the concrete target (see Table 2 and Figure 3 for reference).

For the perforation **test 1** ($V_i = 333m/s$ on H300mm target): the velocity and penetration depth profiles for saturated and dry conditions are compared in Fig. 13. Even though the sample is completely perforated, this figure gives us an indication of the projectile position at a given time. We can observe from the velocity profile that during the first phase (T $< 0.5ms$), and unlike the KST-DFH model [17], both saturated and dry concrete behave similarly. This phase is followed by a slightly greater deceleration in dry concrete, leading to a lower residual velocity of the projectile (Fig. 13(a)). This also can be observed from the penetration depth, as the projectile in the saturated sample penetrates deeper than the projectile in the dry sample at a given time (Fig. 13(b)).

Post-processing results in terms of local shear stress at $0.5ms$ for both dry and saturated concrete are shown in Fig. 14. The results suggest that the dry concrete exhibits more intense damage patterns and higher shear stress levels compared to the saturated concrete. This is likely due to the fact that dry concrete has lower tensile strength, which means it is more prone to cracking and fracturing under stress. As a consequence, this model predicts that the perforation of a thin concrete slab is barely affected by the saturation ratio of the material.

For the penetration **tests 2** and **3** ($V_i = 347m/s$ and $227m/s$ respectively on H800mm target): the measured and predicted penetration depths as a function of projectile striking velocity are compared under dry and saturated target conditions (Fig. 15). The prediction shows a trend of slightly underestimating the penetration depth as the striking velocity increases. We can observe that the penetration depth obtained in the test with $V_i = 347m/s$ is greater than that of $V_i = 227m/s$. Therefore, the influence of initial velocity of projectile on the penetration depth of projectile has been satisfactorily captured by the numerical simulations: penetration depth increases with the initial velocity of projectile. Additionally, it has been shown that the projectile penetration processes depend significantly on the free water content of the concrete structure. As the water content decreases, the penetration of projectile into the concrete structures becomes more difficult because dry concrete possesses a greater failure stress and more significant pore closing, thus it becomes very challenging

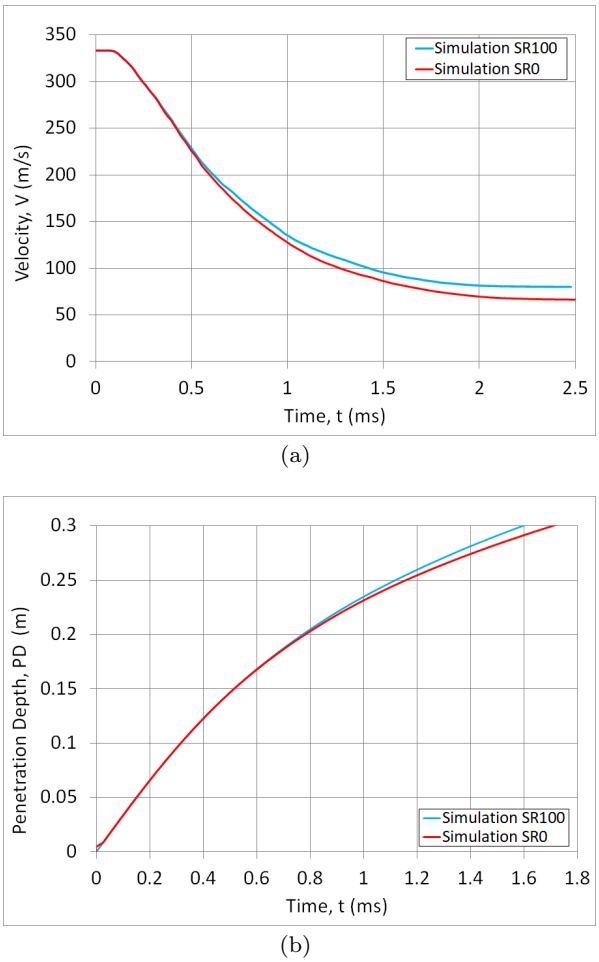

Fig. 13 Test 1 simulation results for saturated and dry target conditions **a** velocity, **b** penetration depth profiles

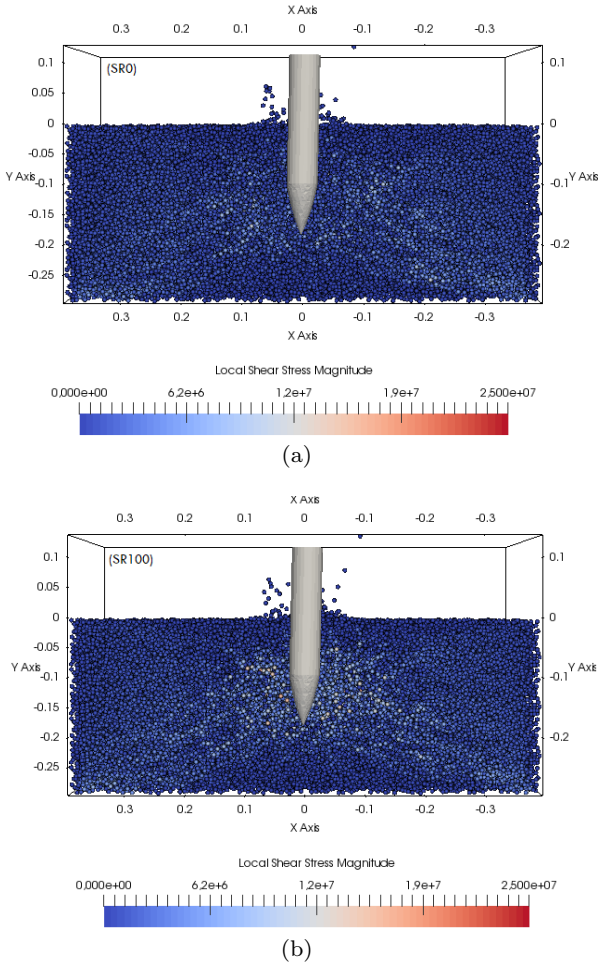

Fig. 14 Test 1 local shear stress magnitude at $0.5ms$ for **a** saturated, **b** dry target conditions

for the projectile to penetrate into the dry concrete target (Fig. 16). The final penetration depth in **tests 2** and **3** for dry concrete is $0.235mm$ and $0.2mm$ respectively.

7 Conclusion

The DE model presented in this paper focuses on modeling the behavior of concrete under dynamic loading at the structural scale. In order to reproduce the effect of strain rate on concrete failure mechanism, the local interaction law validated in a previous study [5] was extended by introducing the dimensionless dynamic load increase factor (DIF) as a function of strain rate. This effect is more pronounced in dynamic strength under tension than under compression. To validate the model, three simulation tests were performed on saturated concrete targets and compared with experimental results. It was shown that the general trend of projectile penetration was correctly reproduced, and that the proposed model is capable of providing a reasonable prediction of the mechanical behavior of saturated concrete subjected to projectile penetration. The study also investigated the effect of saturation ratio on the be-

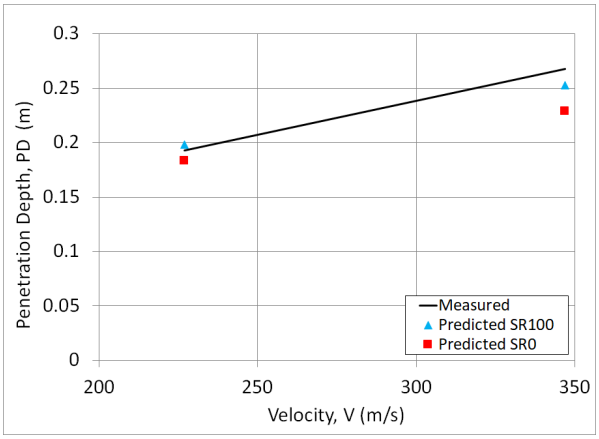

Fig. 15 Tests 2 and 3 measured versus predicted depth of penetration as a function of striking impact velocity for saturated and dry target conditions at $1.4ms$

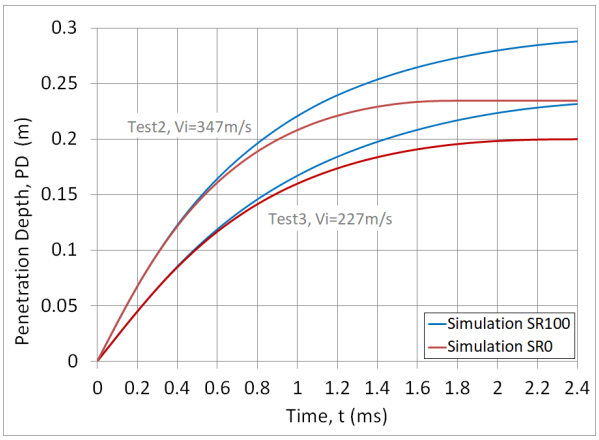

Fig. 16 Tests 2 and 3 simulation results for saturated and dry target conditions: penetration depth profiles

havior of concrete structures under impact in a purely predictive way. While the model proposed in the first paper [5] considers the effect of saturation ratio, it does not account for its relationship with the strain rate effect. Therefore, a calibration of the DIF parameters for both dry and saturated concrete was conducted. The results indicate that dry concrete exhibits higher penetration resistance compared to saturated concrete, where shear stresses dominant over compression and tension stresses. In other words, the reduction of free water content in concrete enhances the influence of the projectile's initial velocity (V_i) on its penetration behavior. The obtained numerical results provide a first estimation of the influence of water content on the penetration performance of concrete targets. In conclusion, this work aimed to address the need for a predictive model capable of determining the depth of penetration of a projectile into concrete. Such a model would enable accurate prediction of penetration depth, which is crucial for a variety of defensive and non-defensive applications. As a perspective, it is important to study the penetrability of various geomaterials, including different kinds of rocks or different types of concrete, and to have a predictive model that only requires conventional laboratory test data for material characterization.

Acknowledgements This research was financially supported by CEA DAM, the Direction of military applications of the French Alternative Energies and Atomic Energy Commission. The authors would also like to acknowledge Dr. Christophe Pontiroli for his scientific advice.

Conflict of interest

The authors declare that they have no conflict of interest.

References

1. Accary A, Malecot Y, Daudeville L (2019) Design and Evaluation of a Deformable Sensor for Interstitial Pore Pressure Measurement in Concrete under Very High Stress Level. Applied Sciences 9(13):2610.
2. Antoniou A, Daudeville L, Marin P, et al (2018) Discrete element modelling of concrete structures under hard impact by ogive-nose steel projectiles. Eur. Phys. J. Spec. Top. 227, 143–154.
3. Baroth J, Briffaut M, Vu D, Malecot Y, Daudeville L (2021) Prediction of perforation into concrete accounting for saturation ratio influence at high confinement. International Journal of Impact Engineering, 156, 103923.
4. Baroghel-Bouny V, Mainguy M, Lassabatere, T, Coussy O (1999) Characterization and identification of equilibrium and transfer moisture properties for ordinary and high-performance cementitious materials. Cement and Concrete Research, 29:1225–1238.
5. Benniou, H, Accary A, Malecot Y, et al (2021) Discrete element modeling of concrete under high stress level: influence of saturation ratio. Comp. Part. Mech. 8, 157–167.
6. Bian H, Jia Y, Pontiroli C, Shao J-F (2018) Numerical modeling of the elastoplastic damage behavior of dry and saturated concrete targets subjected to rigid projectile penetration. Int J Numer Anal Methods Geomech. 42: 312–338.
7. Bischoff PH, Perry SH (1991) Compressive behavior of concrete at high strain rates. Materials and Structures, 24(6):425–450.
8. CEB-FIP model code 1990. Comité Euro international du Béton. Ed. Thomas Telford.
9. Chen X, Fan S, Li Q (2008) Oblique and normal perforation of concrete targets by a rigid projectile. International Journal of Impact Engineering, 30:617–637.
10. Daudeville L, Malecot Y (2011) Concrete structures under impact. European Journal of Environmental and Civil Engineering, 15(sup1):101–140.
11. Donze F, Magnier S, Daudeville L, Mariotti C, Davenne L (1999) Numerical study of compressive behavior of concrete at high strain rates. ASCE Journal of Engineering Mechanics, 125(10):1154– 1163.
12. Dupray F, Malecot Y, Daudeville L (2010) Experimental behaviour of high-performance concrete in confined tension. Materials and structures, 43, 699-707.
13. Erzar B, Forquin P (2010) An experimental method to determine the tensile strength of concrete at high rates of strain. Experimental Mechanics, 50(7):941–955.
14. Erzar B, Forquin P (2014) Analysis and modeling of the cohesion strength of concrete at high strain-rates. International Journal of Solids and Structures, 51(14), 2559-2574.
15. Forquin P, Hild F (2008) Dynamic fragmentation of an ultra-high strength concrete during edge-on impact tests. Journal of Engineering Mechanics, 134(4):302–315.
16. Forquin P, and Hild F (2010) A probabilistic damage model of the dynamic fragmentation process in brittle materials. Advanced applied mechanics,44:172.
17. Forquin P, Sallier L, Pontiroli C (2015) A numerical study on the influence of free water content on the ballistic performances of plain concrete targets. Mechanics of Materials, 89:176–189.
18. Frangin E, Marin P, Daudeville L (2006) On the use of combined finite/discrete element method for impacted concrete structures. Journal de Physique IV, 134: 461-466.
19. Gabet T, Vu X. H, Malecot Y, Daudeville L (2006) A new experimental technique for the analysis of concrete under high triaxial loading. Journal de Physique IV, 134: 635-640

20. Gabet T, Malecot Y, Daudeville L (2008) Triaxial behavior of concrete under high stresses: Influence of the loading path on compaction and limit states. Cement and Concrete Research, 38(3):403–412.
21. Hentz S (2003) Modélisation d'une Structure en Béton Arm Soumise un Choc par la méthode des Eléments Discrets. PhD thesis, Université Joseph Fourier.
22. Kozicki J, Donze F (2009) YADE OPEN DEM: an open-source software using a discrete element method to simulate granular material. Engineering Computations 26(7):786–805.
23. Kristoffersen M, Toreskås O.L, Dey S, Børvik T (2021) Ballistic perforation resistance of thin concrete slabs impacted by ogive-nose steel projectiles. International Journal of Impact Engineering, 156, 103957.
24. Li Q, Reid S, Wen H, Telfordc A (2005) Local impact effects of hard missiles on concrete targets. International Journal of Impact Engineering, 32(1-4):224–284.
25. Malecot Y, Daudeville L, Dupray F, Poinard C, Buzaud E (2010). Strength and damage of concrete under high triaxial loading. European Journal of Environmental and Civil Engineering, 14(6-7): 777-803.
26. Malecot Y, Zingg L, Briffaut M, Baroth J (2019) Influence of free water on concrete triaxial behavior: The effect of porosity. Cement and Concrete Research, Volume 120, Pages 207-216.
27. Malvar L, Crawford, JE, Wesevich JW, Simons D (1997) A plasticity concrete material model for DYNA3D. International journal of impact engineering, 19(9-10): 847-873.
28. Malvar L, Ross C (1998) Review of strain rate effects for concrete in tension. Materials Journal, 95(6):735–739.
29. Malvar L, Crawford, John E (1998) Dynamic Increase Factors for Concrete. Twenty-Eighth DDESB Seminar Orlando, FL, August 98.
30. Piotrowska E, Malecot Y, Ke Y (2014) Experimental investigation of the effect of coarse aggregate shape and composition on concrete triaxial behavior. Journal of Mechanics of Materials, 79:45–57.
31. Poniard C, Piotrowska E, Malecot Y, Daudeville L, Landis E (2012) Compression triaxial behavior of concrete: the role of the meso-structure by analysis of x-ray tomographic images. European Journal of Environmental and Civil Engineering, 16 (supp. 1):115–136.
32. Pontiroli C, Erzar B, Buzaud E (2014) Concrete behavior under ballistic impacts: Effects of materials parameters to penetration resistance and modeling with PRM model. Computational Modelling of Concrete Structures, 2:685–693.
33. Pontiroli C, Rouquand A, Mazars J (2004) Predicting concrete behavior from quasi- static loading to hypervelocity impact. an overview of the PRM model. European Journal of Environmental and Civil Engineering, 14(6-7):703–727.
34. Rossi P, Van-Mier J, Toutlemonde F, Le-Maou F, Boulay C (1994) Effect of loading rate on the strength of concrete subjected to uniaxial tension. Materials and Structures, 27(5):260– 264.
35. Schuler H, Mayrhofer C, Thoma K (2006) Spall experiments for the measurement of the tensile strength and fracture energy of concrete at high strain rates. International Journal of Impact Engineering, 32(10):1635–1650.
36. Shiu W, Donze F, Daudeville L (2008) Compaction process in concrete during missile impact: a DEM analysis. Computers and Concrete, 5(4): 329-342.
37. Vu XH, Malecot Y, Daudeville L, Buzaud E (2009) Experimental analysis of concrete behavior under high confinement: effect of the saturation ratio. International Journal of Solids and Structures, 46:1105–1120.
38. Vu XH, Malecot Y, Daudeville L (2009) Strain measurements on porous concrete samples for triaxial compression and extension tests under very high confinement. The Journal of Strain Analysis for Engineering Design, 44(8):633-657.
39. Vu XD, Briffaut M, Malecot Y, Daudeville L, Ciree B (2015). Influence of the saturation ratio on concrete behavior under triaxial compressive loading. Science and Technology of Nuclear Installations, 2015, Article ID 976387.
40. Zukas J (1992) Penetration and perforation of solids. Krieger Publishing Co.